ASEAN Journal of Chemical Engineering 2023, Vol. 23, No. 1, 62 – 76

Statistical Characterization of Bubble Breakup Flow Structures in Swirl-Type Bubble Generator Systems

Drajat Indah Mawarni*[,1,2]
Wibawa Endra Juwana*[,3]
IGNB. Catrawedarma*[,4]
Kumara Ari Yuana*[,5]
Wiratni Budhijanto*[,6,7]
Deendarlianto*[,1,7]
Indarto*[,1,7]
[1] *Department of Mechanical and Industrial Engineering, Faculty of Engineering, Universitas Gadjah Mada, Grafika 2 Street, Yogyakarta 55281, Indonesia*
[2] *Department of Mechanical Engineering, Akademi Teknologi Ronggolawe Cepu, Kampus Ronggolawe Street, Block B No.1 Mentul, Cepu 58315, Indonesia*
[3] *Department of Mechanical Engineering, Faculty of Engineering, Universitas Sebelas Maret, Ir. Sutami Street No.36A, Surakarta, Indonesia*
[4] *Department of Mechanical Engineering, Politeknik Negeri Banyuwangi, Raya Jember Km. 13 Street, Labanasem, Banyuwangi 68461, Indonesia*
[5] *Computer Science Departement, Universitas Amikom Yogyakarta, Jl Raya Pajajaran, Ring Road Utara, Sleman, Yogyakarta, Indonesia*
[6] *Bioprocess Engineering Research Group, Department of Chemical Engineering, Faculty of Engineering, Universitas Gadjah Mada, Grafika 2 Street, Yogyakarta 55281, Indonesia*
[7] *Center for Energy Studies, Universitas Gadjah Mada, Sekip K-1A UGM Campus, Yogyakarta 55281, Indonesia*
[*] *e-mail: drajatindah74@mail.ugm.ac.id*

Submitted 27 October 2022 *Revised* 13 December 2022 *Accepted* 26 December 2022

Abstract. The bubble breakup pattern on a swirl-type bubble generator (MBG) with water and air fluids was experimentally studied. The bubble breakup pattern was analyzed visually and characterized using several parameters such as Pressure Drop (ΔP), Kolmogorov Entropy, Standard Deviation, and DWT (Discrete Wavelet Transform), which were taken from the extraction of pressure signals at the water inlet and outlet of the bubble generator. The wavelet spectrum of the measured signal was shown to identify the overall bubble breakup pattern, and the wavelet variance vector is proposed as a character vector to identify the bubble breakup pattern. The results show that there were three types of different flow breakup patterns: (1) static breakup, (2) dynamic breakup, and (3) tensile breakup. The observed bubble breakup sub-patterns can be categorized into tensile, moderate tensile, high tensile, dynamic, low dynamic, static, and high static sub-patterns. The static clustered breakup pattern has the highest wavelet energy compared to the tensile and dynamic clustered breakup.

Keywords: Bubble breakup, swirl, pressure drop (ΔP), standard deviation, Kolmogorov entropy, discrete wavelet transform (DWT), static breakup, dynamic breakup, tensile breakup

DOI: 10.22146/ajche.78558

INTRODUCTION

The Swirl-type MBG is an MBG that can produce small bubbles, which is currently being developed. In addition to having the ability to produce small air bubbles effectively, the design is also simpler with an easier manufacturing process (Tabei & Haruyama. 2007, Terasaka et al. 2011, Kogawa et al. 2015, Xu et al. 2018) compared to the non-Swirl-type MBG.

Some researchers suggest that swirl flow can increase the turbulence of the liquid to increase bubble breakup (Tabei & Haruyama. 2007, Juwana et al. 2018, Huang et al. 2019, Mawarni et al. 2022). In particular, the turbulent flow was used to break the main air bubbles into cluster microbubbles, as reported in the jet-type MBG (Shuai et al. 2019a, Shuai et al. 2019b) and venturi-type MBG (Huang et al. 2019).

In general, there are three methods to generate swirl flow, namely: active technique, passive technique, and a combination of active and passive techniques (Bergles. 1997). The active method requires an active power supply, while the passive method does not require a power supply. Previously, it was also conveyed by Islek (2004) that the method to produce swirl flow can use a rotating flow guide (vane guide), inlet tangential flow injection, rotating pipe (pipe rotation), or a swirl generator. According to Chen et al. (2016), the passive methods include the guided vanes and swirl or tangential inlet cylinders.

In this experiment, producing swirling flow was done using a passive technique method, specifically by making a tangential inlet channel because this method has an easy and simpler design than other methods. Unlike the swirl-type MBG with the tangential inlet method used by Tabei & Haruyama (2007). In this experiment, the air nozzle can be adjusted back and forth, so that the size of the resulting bubble diameter can be adjusted to its desirable sizes.

Currently, research on MBG is more focused on the bubble breakup mechanism and the visualization of bubble breakup patterns in the swirl flow area, especially on the characteristics of the swirl flow area (Xu et al. 2018, Liu & Bai. 2019) and gas-liquid separation applications (Yin et al. 2015, Yin et al. 2018). A number of researchers had conducted research to observe bubble breakup events. Song et al. (2019) conducted an experiment to observe the occurrence of bubble breakup on a venturi type bubble generator and divided it into three bubble flow breakup patterns through visualization, namely: a bubble breakup pattern along the direction of movement, a swirling bubble pattern which then breaks into two child bubbles, and a burst bubble pattern into a number of sub-bubbles directly (Zhao et al. 2018). Zhao et al. (2019) conducted a visual experiment by illustrating the movement and bubble breakup process in a Venturi-type MBG to observe the bubble formation in the rectangular Venturi channel to obtain bubbles of small size. Xu et al. (2018) designed a planar cyclone for visualization of bubbles in a degassing hydrocyclone cross-section. The pressure distribution was studied through a series of experiments and simulations. Bubble dynamics were simulated through Euler-Euler and Euler-Lagrange approaches, and the results were compared with the imaging results. Liu et al. (2018) investigated the coalescence and breakup of non-aqueous oil droplets in a rotating flow area to separate water and oil, and Wang et al. (2020), visually observed and simulated

CFD of three different bubble breakup patterns on swirl-venturi type MBG, which are tensile breakup, erosive dynamic breakup, and erosive static breakup.

The visual analysis conducted by previous researchers to identify flow patterns/bubble breakup patterns has a high degree of subjectivity because it gives different results when observed by other researchers. Hence, it is required to construct a more sophisticated method, namely by using data on pressure signal fluctuations. The identification of bubble breakup patterns and acquiring statistical parameters of pressure signal fluctuations from each pattern using wavelet analysis are the novel approaches in this field. In addition to its simple construction, this analysis method is also non-intrusive.

In this study, pressure signal fluctuations were processed and examined by DWT (Discrete Wavelet Transform) to detect or describe bubble breakup patterns. DWT is a multi-resolution decomposition method to construct a good local description signal in the time domain and frequency domain simultaneously. As stated by Elperin & Klochko. (2002), Wijayanta et al. (2022), Astyanto et al. (2022), and Catrawedarma et al. (2020), DWT can provide a signal break down time scale which is an intermediate between the frequency and time domains. The certain characteristic of the fundamental wavelet function enables to obtain a confine distribution of signal energy through frequency octaves that gives a small size of the feature vector. This is very convenient, if the Fourier spectrum is relatively featureless, so that it can describe a movement pattern. Based on the algorithm proposed and experiments conducted by Wijayanta et al. (2022), Astyanto et al., (2022), and Catrawedarma et al. (2020), the whole-scale energy wavelet distribution can be handled as a breaks down of the signal variance into a scale, so that the entire-scale energy distribution can be used as an measurement of the flow pattern.

Even though many researchers have identified a two-phase gas-liquid flow pattern, no one has yet identified a bubble breakup pattern on the Swirl-type MBG using the DWT analysis of pressure signal fluctuation data. Referring to the existing knowledge gap, in this study, the author will provide a contribution knowledge of various bubble breakup patterns on MBG Swirl which are rarely found in the existing open literature to determine the bubble breakup pattern of swirl-type MBG which is observed visually. The pattern is characterized by pressure drop, standard deviation, discrete wavelet transforms (DWT), and entropy of Kolmogorov that are taken from the extraction of pressure signal fluctuations at the water inlet and MBG outlets.

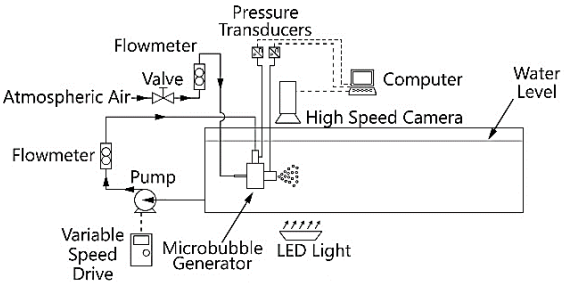

Fig. 1: The apparatus diagram of the MBG Swirl type.

MATERIALS AND METHODS

The active fluid used were air as a gas fluid and water as a liquid fluid. The research data set is provided in Table 1 while the illustrative diagram of the experimental equipment utilized in this research is shown in Fig. 1.

Table 1. Research data matrix.

Microbubble Swirl Generator		
Water flow rate (Q_L) ($l\ min^{-1}$)	Air flow rate (Q_G) ($l\ min^{-1}$)	Air nozzle distance (ℓ) (m)
30 – 70	0.1 – 1	0.001

In this experimental study, the water entered through a tangential inlet channel, which was in one of the pipe walls forming a swirling flow as shown in Fig. 2. with the increasing of tangential momentum to axial momentum (swirl number), the tangential velocity and turbulence intensity increase significantly, in which it causes lower pressure at the center of the whirlpool, (Mawarni et al. 2022). The abrupt contraction in the mixing channel causes the degreasing of the water pressure under atmospheric pressure so that the air was absorbed automatically. The axial direction of the airflow was broken up by the water flow with very high turbulence intensity forming a bubbly flow in the mixing channel and it breaks due to sudden enlargement at the MBG outlet.

The high-speed camera was used to record the video of the bubble breakup pattern while the pressure tap is used to set the pressure signal. A high-speed Phantom Miro 310 camera with a resolution and frame rate of 1280 × 800 and 3000 fps, respectively, was used to record video of the bubble breakup pattern. The distance between the test part and the camera lens was set to a distance of 350 mm, which was also done by Juwana et al. (2019). A series of LED lights to even out the lights were emitted from behind to capture the best images. The difference in pressure at the inlet and outlet of MBG was measured by a pressure transducer Valydine P55D with a capacity of 55 kPa and an accuracy of ±0.25%., which was connected to an analog to digital converter (ADC) to be converted into digital data, then recorded by a personal computer. The data acquisition Advantech USB4716 was used to convert analog to digital signals and stored on personal computer at 1000 samples for one second. Construction and operation details of DPT connected to Advantech USB4716 data acquisition was as described by Catrawedarma et al. (2021).

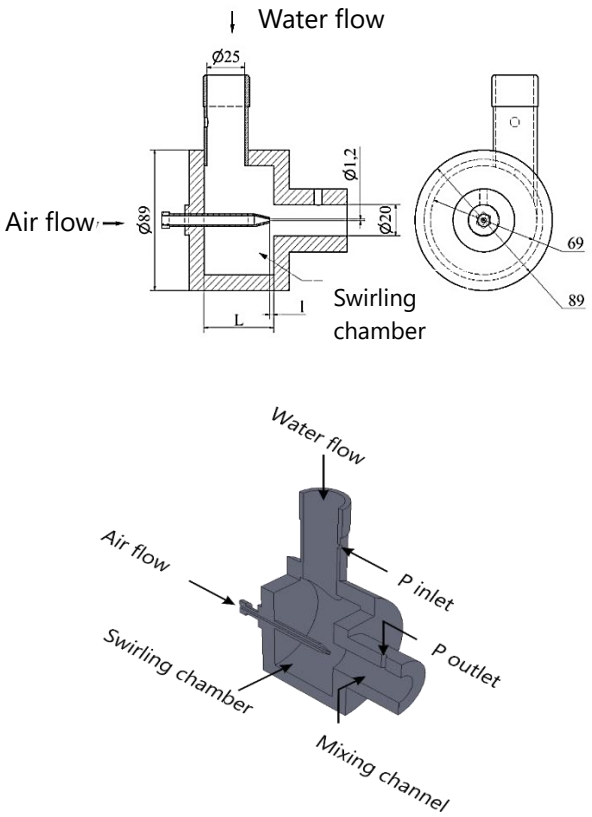

Fig. 2: Swirl-type MBG.

The bubble breakup flow pattern video and pressure signal fluctuation in the cross-sectional test were recorded simultaneously. Time series from pressure signal fluctuation processed using a wavelet transform. Time domain pressure signals were processed using the wavelet toolbox in the MATLAB software to obtain some of the detail and the approximate signals as well as the variants of each detail, and the approximate scale that represents the wavelet energy.

RESULTS AND DISCUSSION

Visual observation

In this study, visual observations were made from video images taken from the experiment. In the range of water (Q_L) and air (Q_G) debit variations with the air nozzle distance (ℓ), three flow breakup patterns can be visually identified.

Experiments at low water flow, 30 l min^{-1}, with variations in air flow from 0.1 to 0.8 l min^{-1} show that the observed bubble breakup pattern was a bubble channel flowing in the mixing channel and the breakup that occurs in sudden enlargement was a breakup tensile. This breakup pattern is characterized by a burst of air bubbles moving along the axial direction, where they experience stretching and deformation. Only when the bubble was stretched to a certain extent, a distinct neck appears, after which the neck shrank and broke up, becoming two or more child bubbles as presented in Fig. 3.

On the other hand, the visual observation on the Q_G ranged from 0.1 to 0.8 l min^{-1} with a constant Q_L of 50 l min^{-1} was a bubble channel in the mixing channel, formed a dynamic breakup pattern in sudden enlargement. In this breakup pattern, the bubbles moved in a radial direction to the geometric center axis, and flow obliquely upward from the center to the wall. During the transfer process, the bubbles deformed badly, causing the neck to shrink, and burst into a cluster of child bubbles. In this pattern, the bubbles burst as it moves, as shown in Fig. 4.

Furthermore, the visual observations in the Q_G ranged from 0.1 to 0.8 l min^{-1} with a constant Q_L of 70 l min^{-1}, the observed flow pattern was a bubble channel flowing in the mixing channel and the breakup pattern that occurs in sudden enlargement was a static breakup. In this breakup pattern, it is indicated by the bubble decelerating (speed reduction), and then deforming after experiencing a sudden enlargement at the bubble generator outlet. Subsequently, the

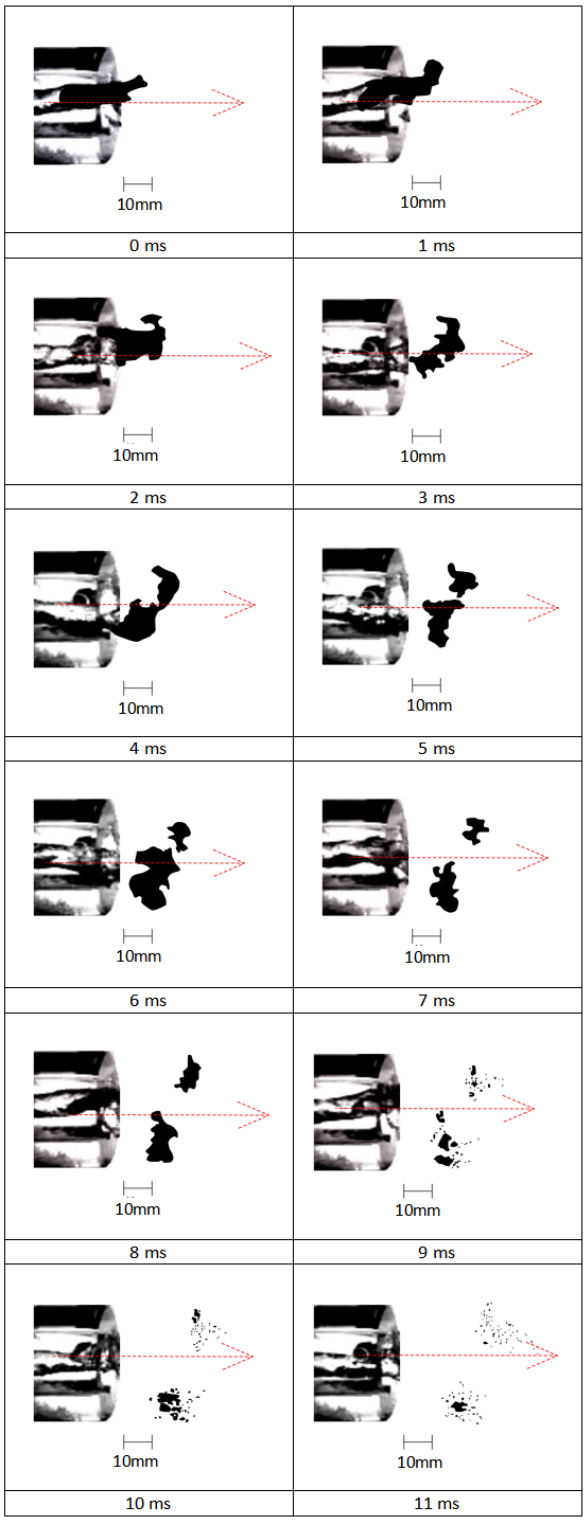

Fig. 3: Breakup tensile visualization.

bubble traveled in a radial direction for a very short distance and stops near the exit of the MBG. Meanwhile, a huge number of small bubbles burst continuously from the main bubble and flowed downstream as shown in Fig. 5.

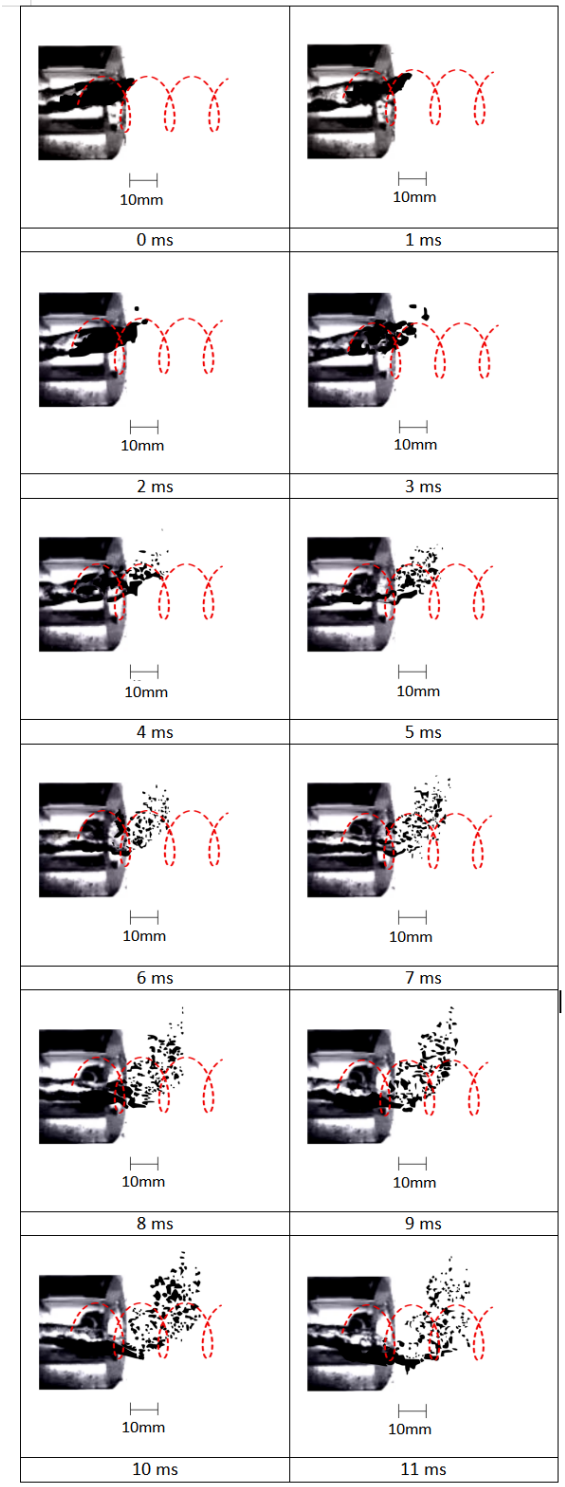

Fig. 4: Dynamic breakup visualization.

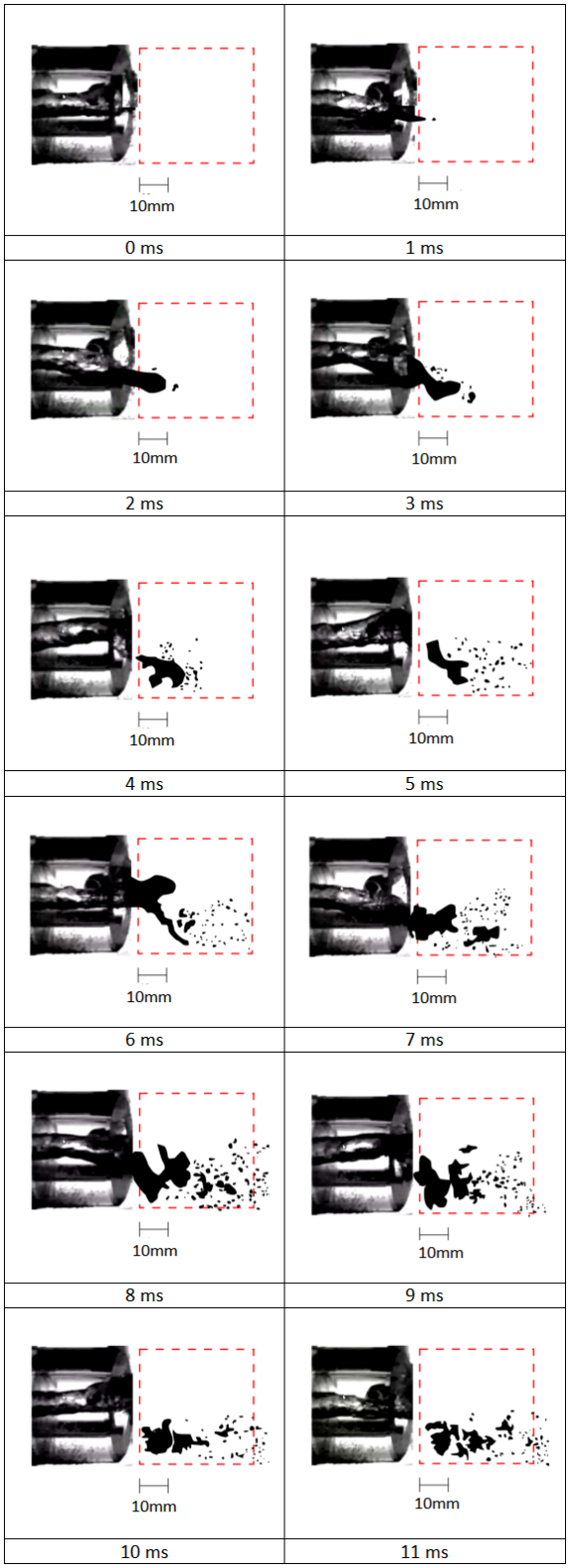

Fig. 5: Static breakup visualization.

Stochastic and Chaotic analysis

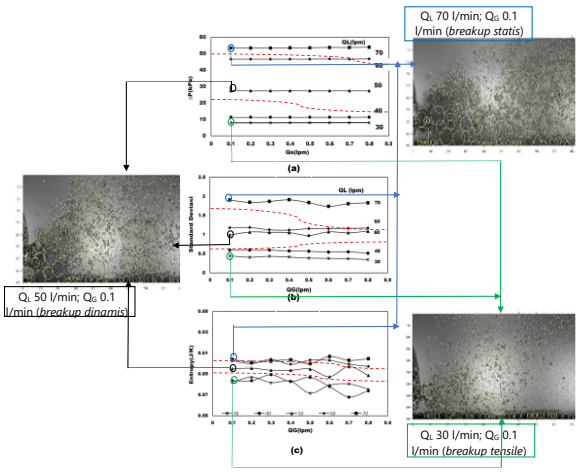

Fig. 6: Photograph, pressure drop(ΔP) (a), standard deviation (b), and entropy Kolmogorov (c) at variation Q_L = (30, 50, 70) l min^{-1} at constant Q_G = 0.1 l min^{-1}.

The effect of Q_L and Q_G on the value of pressure drop (ΔP) (a), standard deviation (b), and Kolmogorov entropy (c), are shown in Fig. 6. The waters momentum in the form of inertial force directly grows the stress of hydrodynamics around the water (liquid) The stress of hydrodynamics force around the water (liquid) is the force which trying to deform (breakup force). The hydrodynamics surface tension attempt to maintain the bubble structure, and the hydrodynamics tension attempt to disrupt the bubble (Huang et al. 2020). If the rehabilitated force is less than the breakup force, then the bubble will burst (Fu & Ishii, 2003). In the same study, they suggest that bubble rupture occurs if the Webber number (hydrodynamic ratio force vs. surface tension) is greater than the critical number. Under specific conditions, when the hydrodynamic pressure is equal to the surface tension, bubbles tend to be able to maintain their shape. Bubbles will burst at high instability levels and collide with other bubbles, coalesce (merge) and form larger bubbles as proposed by Mote (1973) and Apazidis (1985). The bubble impact takes place due to various factors, including turbulence due to random bubble movement, dissimilarities of Buoyancy forces due to dissimilarities of bubble size, and laminar shear forces caused by the position of bubbles at high or low water (liquid) velocities (McBride et al. 1981). Nevertheless, if the hydrodynamic tension around the water (liquid) exceeds the surface tension, the bubble will break into smaller bubbles.

The stochastic analysis consists of the mean of pressure drop (ΔP) and standard deviation as a function of Q_L and Q_G. Fig. 6(a) shows the relationship between ΔP and Q_G and Q_L, indicating that the higher the value of Q_L, the more ΔP increases significantly, while the higher the value of Q_G, the more ΔP increases, but not significantly. This is due to the effect of hydrostatic pressure and the influence on friction loss during coalescence and breakup (Huang et al. 2020). In this study, liquid fluid has a greater hydrostatic pressure and effect on friction loss than gas fluid because of the longer passing distance of liquid fluid compared to the passing distance traveled by gas fluid. The standard deviation is shown in Fig.6 ΔP, which illustrates the average amplitude of pressure drop in the test section. The observed phenomenon can be divided into 3 regions (categories) depending on the amplitude and conditions of Q_L and Q_G. For Q_L 30 and 40 l min^{-1}, representing the tensile breakup category, the amplitude tends to be constant as the Q_G increases. On the other hand, as for the water discharges of 50 and 60 l min^{-1}, representing the dynamic breakup category, the amplitude increased with increasing Q_G, and at Q_L 70 l min^{-1}, representing the static breakup category, the amplitude increased more significantly with the increasing Q_G. Following Xiang et al. (2017), the average pressure drop

amplitude depends on the distribution and dimensions of the bubble. The amplitude of the pressure oscillation is higher when the bubble distribution is random, and the size of the bubble is larger. The bubble size and its location will affect the near-wall pressure. The larger the bubble size and the nearer its position to the wall, the more significant the effect on the near-wall pressure. Furthermore, the oscillation of water movement due to the movement of bubbles in liquid has a great effect on pressure oscillation, as stated by Catrawedarma et al. (2021).

The chaotic systems are identified by a measurement of uncertainty (the rate of development of small perturbation) identified by the entropy of Kolmogorov (Vial et al, 2000) where the computation iterations are addressed by Grassberger (1983) and Catrawedarma et al. (2021). Fig. 6(c) illustrates the relationship between entropy and Q_L and Q_G. In Fig. 6(c), it can be seen that the tensile breakup pattern, represents low water discharge of (30-40) l min^{-1} with a Q_G variation of (0.1-0.8) l min^{-1}, and the dynamic breakup pattern represents water discharge of (50-60) l min^{-1}, while the static breakup pattern represents water discharge of 60 l min^{-1} at Q_G 0.7-0.8 l min^{-1} and water discharge of 70 l min^{-1} for Q_G (0.1-0.8) l min^{-1}. In the tensile breakup pattern, entropy tends to change as Q_G increases. This is due to the influence of the number and size of bubbles that increase as the Q_G increases. Meanwhile, the irregular rotating motion of the bubbles during a dynamic breakup can increase the hydrodynamic pressure around the liquid, so that the rupture, collision, and merging of bubbles occurred more frequently, leading to an escalation of the chaotic system. In the static breakup pattern, entropy increases because the bubbles break into smaller sizes as a result of increased chaotic activity. The contortion movement of the bubbles makes the incremental on entropy in the static breakup pattern.

Wavelet transforms

Wavelet analysis was also used as an additional inspection to characterize the liquid movement design. The inspection of the wavelet breaks down the primary waves into discretized and scaled versions. On the broke down wave, the frequency range is reduced, but the scale captured by the signal is increased. Discrete wavelet transform was used in this study to divide the original signal into approximation and detail. On the other hand, Daubechies 4 wavelets were used to break down the wave into eight levels. The method of Daubechies viable obtaining favorable ranges of data to compute the median and deviation due to it uses the scalar product by scaling wavelet and the signal to compute the moving average and difference (Catrawedarma et al. 2021, Morshed et al. 2020). The determination of the maximum decomposition level has been clearly reported by Ephrin and Klochko (2002). The primary signal breaks down into eight details and approximations is shown in Fig. 7. In this wavelet patterns, d1 possesses the most detailed scale under the biggest frequency band, while d2, d3, etc., have fewer frequencies, and a8 have the large-scale approximation with low frequencies.

In this research, the authors emphasized on d6 to comprehend the oscillations due to the movement of air bubbles. The value of d6 represents a high-scale low-frequency signal. High-frequency oscillations are expected because of the effect of bubble rupture and merged frequencies, and the high-scale low-frequency would increase add the continuous flow of surface signals, as addressed by Jana et al. (2006) and Catrawedarma et al. (2021).

In addition, each scale of the variant distribution reflecting the wavelet energy was employed to explain the energy fluctuation of the dynamic process of a particular flow pattern, as shown in Fig. 8. to 10., column (b).

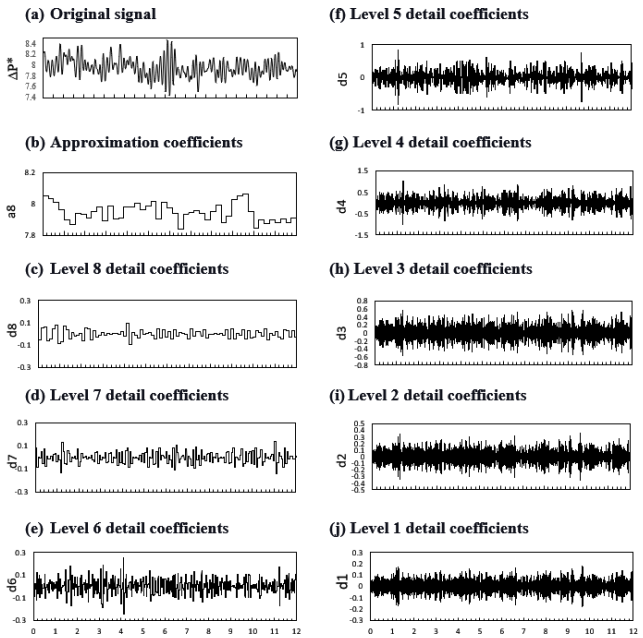

Fig. 7: Wavelet analysis type of MBG *Swirl* at Q_L=30, Q_G=0.1 l min^{-1} at 1 mm air nozzle distance.

Fig. 8-10 are the wavelet analysis with the variation of Q_G values at Q_L = (30, 50, and 70) l min^{-1} with an air nozzle distance of 1 mm. In general, it is known that at increasing Q_L, more bubbles are produced so there are higher frequency fluctuations. Meanwhile, with the escalation of Q_G, the number of bubbles produced also increased although not too significant. These bubbles have a high buoyant force that is used to resist gravity and create fluctuations in the movement of the interface. When Q_L and Q_G are low, the frequency fluctuations and interface movement are relatively smooth because fewer bubbles are generated as stated by Catrawedarma et al. (2021). In Fig. 8 with a constant Q_L of 30 l min^{-1}, there is a tendency to experience air bubble rupture events by forming clustered breakup tensile.

Based on the wavelet energy (column (c)), the clustered breakup tensile was indicated by the peak occurring at d4 and followed by d6-d8 values tends to stabilize at low wavelet energy values. This happens for all variations of Q_G values. In clustered breakup tensile, there were patterns of tensile, moderate tensile, and high tensile. In moderate and high tensile patterns, the peak occurs at d4 followed by a peak at d,5 and tends to be uniform. Compared to tensile patterns, moderate tensile and high tensile patterns have higher wavelet energy values. This is because moderate tensile and high tensile patterns are found at Q_L 40 l min^{-1} with varying Q_G values, where the number of bubbles produced is greater.

In Fig. 9 under constant Q_L of 50 l min^{-1} and varying air discharge, the air bubbles tend to break up by forming dynamic clustered breakups. From wavelet energy (column (c)), the dynamic clustered breakup is shown that the peak occurs at d4 with higher wavelet energy than a tensile clustered breakup and is followed by d6-d8 values that tend to stabilize at low wavelet energy values. In dynamic clustered breakup there are dynamic and low dynamic patterns. The dynamic pattern occurs at a water discharge of 50 l min^{-1} at all variations of air discharge (0.1-0.8) l min^{-1}, while the low dynamic pattern occurs at a water discharge of 60 l min^{-1} with a variation of air discharge (0.1-0.6) l min^{-1}. Meanwhile, at a water discharge of 60 l min^{-1} with a variation of air discharge (0.7-0.8) l min^{-1}, a static pattern occurs with a peak at d4 followed by a peak at d3 then followed by d5.

No	Q_G	Visual (a)	d6 (b)	Wavelet Energy (c)
1	0.1	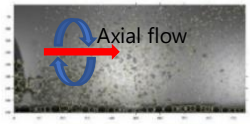	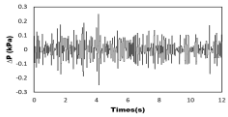	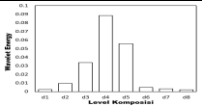
2	0.2	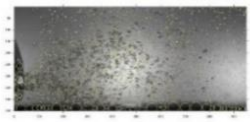	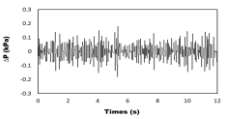	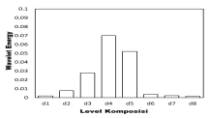
3	0.3	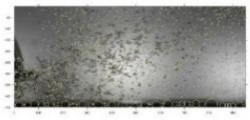	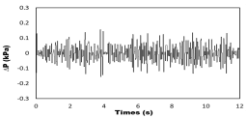	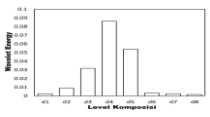
4	0.4	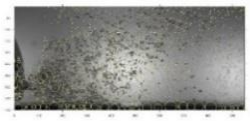	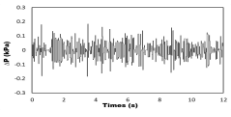	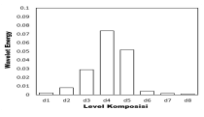
5	0.5	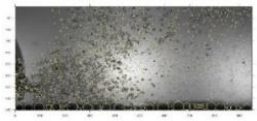	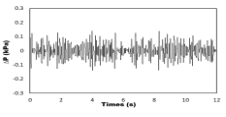	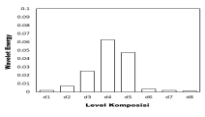
6	0.6		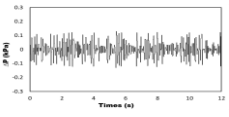	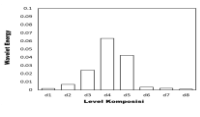
7	0.7	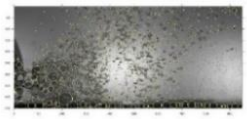	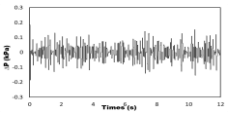	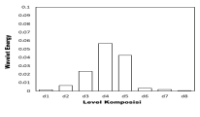
8	0.8	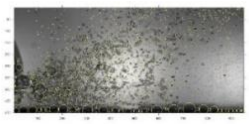	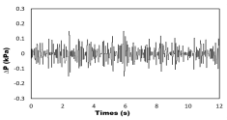	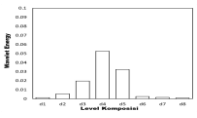

Fig. 8: *Wavelet analysis* results at a water flow rate of 30 l min^{-1} with the variation of air discharge in the MBG at an air nozzle distance of 1 mm.

Fig. 10 shows the constant Q_L of 70 l min^{-1} and the variation of air discharge. It tends to experience air bubble breakup events by forming static clustered breakups. The resulting sub-bubbles separate continuously, and the distribution was more dispersed compared to the dynamic clustered breakup. From the wavelet energy (column (c)), the static clustered breakup was indicated by a peak occurring at d4 and followed by d6-d8 values that tend to stabilize at low wavelet energy values. The static clustered breakup pattern has the highest wavelet energy compared to the tensile and dynamic

clustered breakup. This is due to the greater number of bubbles produced. Therefore, referring to the statement of Catrawedarma et al. (2021), it is generally accepted that with increasing Q_L, more bubbles are produced, creating higher frequency fluctuations. Meanwhile, with the increase of Q_G, the number of bubbles produced also increases although not too significant. In a static clustered breakup, there are static and high static patterns and in the high static pattern, the peak occurs at d4 with a higher energy value than the static pattern.

No	Q_G	Visual (a)	d6 (b)	Wavelet Energy (c)
1	0.1	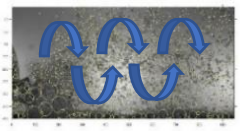	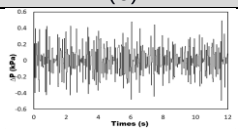	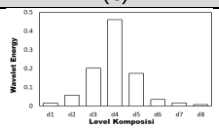
2	0.2	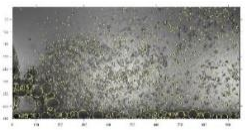	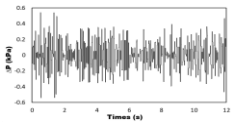	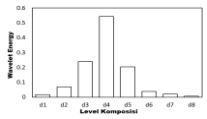
3	0.3	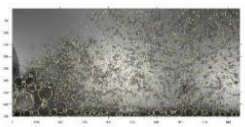	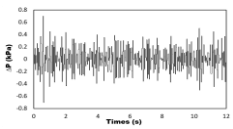	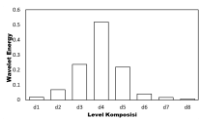
4	0.4	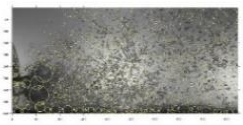	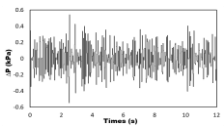	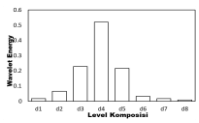
5	0.5	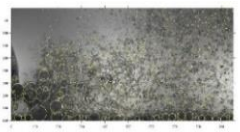	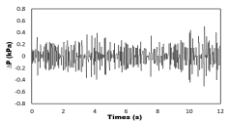	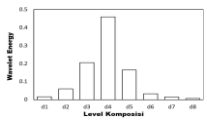
6	0.6	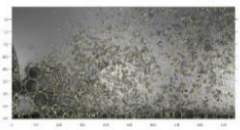	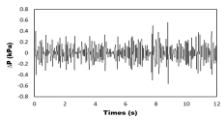	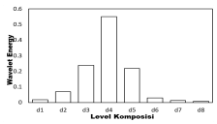
7	0.7	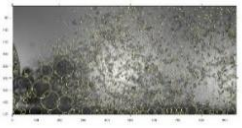	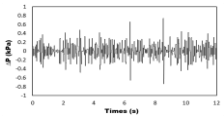	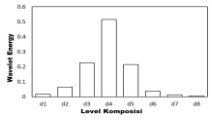
8	0.8	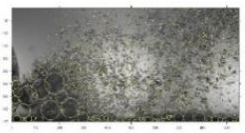	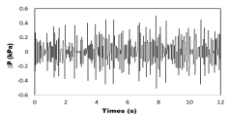	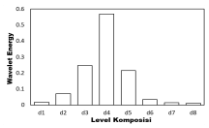

Fig. 9: Example of wavelet analysis results at 50 l min^{-1} water discharge with variation of air discharge in MBG at 1 mm air nozzle distance.

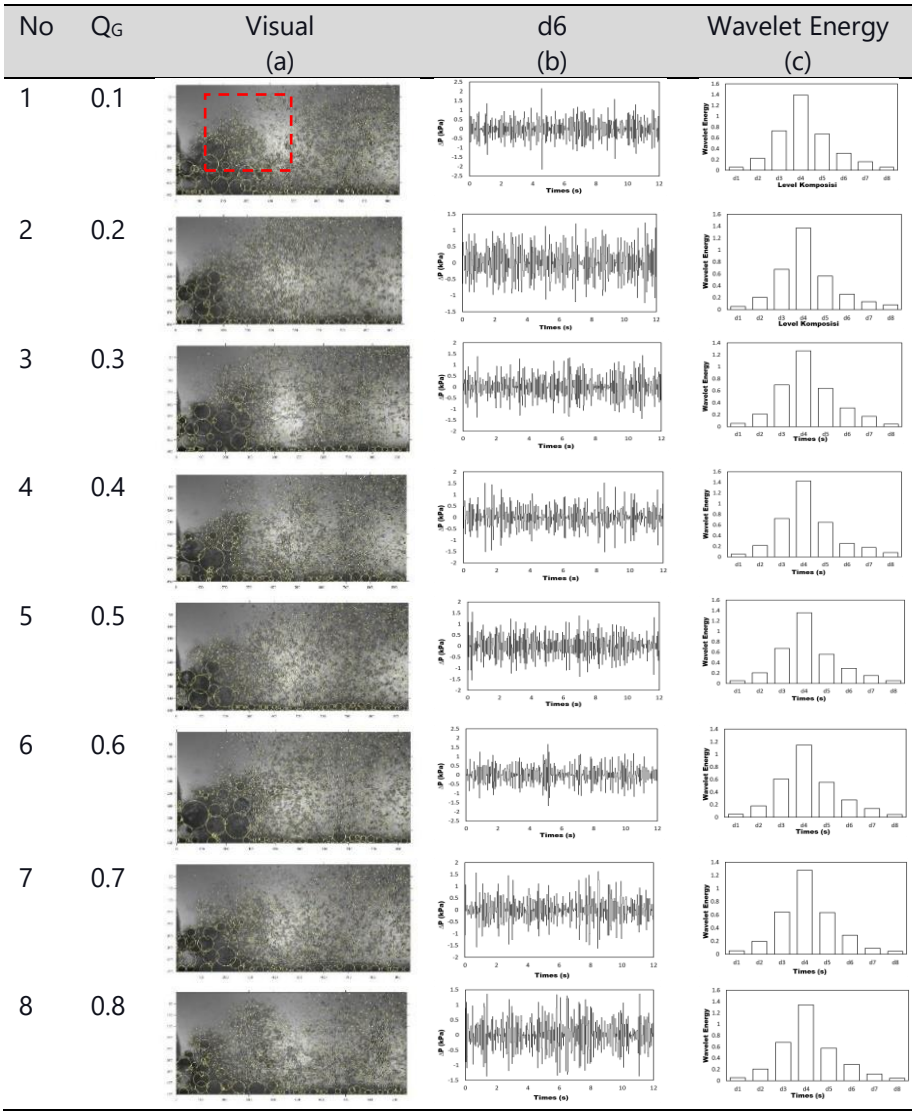

Fig. 10: Example of *wavelet analysis* results at a water flow rate of 70 l min^{-1} with variations in air discharge in the MBG at an air nozzle distance of 1 mm.

Flow pattern map

The bubble breakup patterns in the study are presented in Fig. 11. The bubble breakup patterns obtained were later compared with the breakup pattern model from the research conducted by Wang et al. (2020). This flow bubble breakup pattern was chosen as a comparison in consideration of the occurrence of bubble breakup in the Venturi Swirl type MBG because it is similar to the experimental data that researchers are now doing.

The visualization results show that there are three different bubble breakup flow patterns, namely: tensile breakup, dynamic breakup, and static breakup as identified by Wang et al. (2020) using Venturi Swirl type MBG. The writers developed the three bubble breakup patterns into sub-patterns of tensile, moderate tensile, high tensile, dynamic, low dynamic, static, and high static as shown in Fig. 11. The development of the bubble breakup pattern is based on variations in water and air discharges.

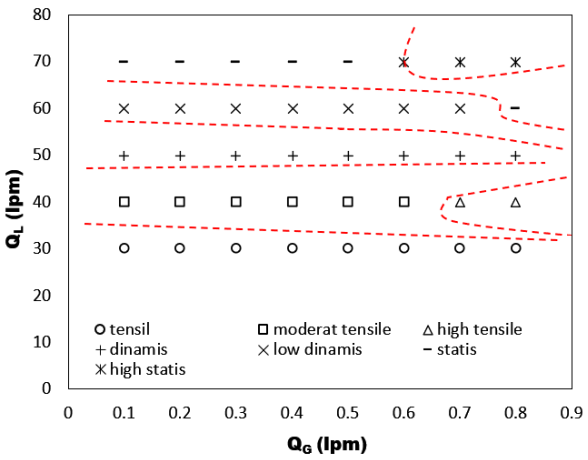

Fig. 11: Bubble breakup pattern in MBG Swirl type

CONCLUSIONS

The bubble breakup pattern of the Swirl-type MBG was investigated using the pressure signal fluctuation. The time series values of the pressure signal fluctuation data were analyzed using the mean pressure drop, the Kolmogorov entropy, a standard deviation of pressure fluctuation, and the discrete wavelet transform (DWT).

The conclusions are as follows:

a) The bubble breakup mechanism at the MBG outlet can be divided into 3 patterns, namely, tensile breakup, dynamic breakup, and static breakup patterns. In addition, it depends on the water and air discharge.

b) As the water flow rate increases, the mean pressure drops, the standard deviation of pressure fluctuation, and the chaotic system increase significantly, while as the air flow rate increases, the increase occured but not significantly.

c) The observed bubble breakup sub-patterns can be categorized into tensile, moderate tensile, high tensile, dynamic, low dynamic, static, and high static sub-patterns.

d) The static clustered breakup pattern has the highest wavelet energy compared to the tensile and dynamic clustered breakup.

ACKNOWLEDGEMENT

This work was carried out in an ongoing research project at the Multiphase Flow Research Group, Fluid Mechanics Laboratory, Mechanical and Industrial Engineering Department Universitas Gadjah Mada, Indonesia. In addition, the authors would like to express the highest gratitude to Chevron Indonesia for the High-Speed Video Camera support. In addition, the authors would like to express the highest gratitude to Chevron Indonesia for the High-Speed Video Camera support.

NOMENCLATURE

Q_L	:	waterflow rate [m^3/s]
Q_G	:	air flow rate [m^3/s]
ℓ	:	air nozzle distance [m]
ΔP	:	pressure drop [Pa]
DWT	:	discrete wavelet transforms
CFD	:	computational fluid dynamic
MBG	:	microbubble generator
LED	:	light emitting diode
ADC	:	analog digital converter
d1, d2, d6	:	level signal decomposition

REFERENCES

Apazidis, N. (1985). Influence of bubble expansion and relative velocity on the performance and stability of an airlift pump. *IJMF*, *11*(4), 459–479.

Astyanto, A. H., Pramono, J. A. E., Catrawedarma, I. G. N. B., Deendarlianto, & Indarto. (2022). Statistical

characterization of liquid film fluctuations during gas-liquid two-phase counter-current flow in a 1/30 scaled-down test facility of a pressurized water reactor (PWR) hot leg. *ANE*, *172*, 109065.

Bergles, A. E. (1997). Heat transfer enhancement-the encouragement and accommodation of high heat fluxes. *JHT*, *119*(1), 8–19.

Catrawedarma, I., Deendarlianto, & Indarto. (2020). The performance and flow characteristics of swirl flow injector type airlift pump system. *AIP Conference Proceedings*, *2248*(July).

Catrawedarma, I. G. N. B., Deendarlianto, & Indarto. (2021). Statistical Characterization of Flow Structure of Air–water Two-phase Flow in Airlift Pump–Bubble Generator System. *IJMF*, *138*, 103596.

Chen, B., Ho, K., Abkar, Y. A., & Chan, A. (2016). Fluid dynamics and heat transfer investigations of swirling decaying flow in an annular pipe Part 2: Fluid flow. *IJHMT*, *97*, 1012–1028.

Elperin, T., & Klochko, M. (2002). Flow regime identification in a two-phase flow using wavelet transform. *EF*, *32*(6), 674–682.

Fu, X. Y., & Ishii, M. (2003). Two-group interfacial area transport in vertical air-water flow - I. Mechanistic model. *NED*, *219*(2), 143–168.

Grassberger, P. (1983). Lim, — 1). *Physical Review*, *28*(4), 2591–2593.

Huang, J., Sun, L., Liu, H., Mo, Z., Tang, J., Xie, G., & Du, M. (2020). A review on bubble generation and transportation in Venturi-type bubble generators. *ECMF*, *2*(3), 123–134.

Huang, J., Sun, L., Mo, Z., Liu, H., Du, M., Tang, J., & Bao, J. (2019). A visualized study of bubble breakup in small rectangular Venturi channels. *ECMF*, *1*(3), 177–185.

Islek, A. (2004). *The Impact of Swirl in Turbulent Pipe Flow*. Retrieved from http://smartech.gatech.edu/handle/1853/4955

Jana, A. K., Das, G., & Das, P. K. (2006). Flow regime identification of two-phase liquid-liquid upflow through vertical pipe. *CES*, *61*(5), 1500–1515.

Juwana, W. E., Widyatama, A., Dinaryanto, O., Budhijanto, W., Indarto, & Deendarlianto. (2019). Hydrodynamic characteristics of the microbubble dissolution in liquid using orifice type microbubble generator. *CERD*, *141*, 436–448.

Kogawa, H., Naoe, T., Kyotoh, H., Haga, K., Kinoshita, H., Futakawa., M. (2015). Development of Microbubble Generator for Suppression of Pressure Wave in Mercury Target of Spallation Source. *JNST*, *52*(12).

Liu, L., & Bai, B. (2019). Flow regime identification of swirling gas-liquid flow with image processing technique and neural networks. *CES*, *199*, 588–601.

Liu, S., Zhang, D., Yang, L. le, & Xu, J. yu. (2018). Breakup and coalescence regularity of non-dilute oil drops in a vane-type swirling flow field. *CERD*, *129*, 35–54.

Mawarni, D. I., Juwana, W. E., Yuana, K. A., Budhijanto, W., Deendarlianto, & Indarto. (2022). Hydrodynamic characteristics of the microbubble dissolution in liquid using the swirl flow type of microbubble generator. *JWPE*, *48*(2), 102846.

McBride, C., Walter, J., Blanch, H. W., & Russell, T. W. F. (1981). Bubble Coalescence and Break-Up in Fermentations. *SEP*, *36*(10), 489-496B.

Morshed, M., Khan, M. S., Rahman, M. A., & Imtiaz, S. (2020). Flow regime, slug frequency and wavelet analysis of air/Newtonian and air/non-Newtonian two-phase flow. *AS (Switzerland)*, *10*(9).

Mote, C. D. (1973). The response of an elastic disk with a moving mass system. *JAMT ASME*, *40*(4), 1151–1152.

Ohnari, H. (1997). Waste water purification in wide water area by use of micro-bubble techniques (article written in Japanese). *JJMF*, *11*(0834), 263–266.

Shuai, Y., Guo, X., Wang, H., Huang, Z., Yang, Y., Sun, J., … Yang, Y. (2019a). Characterization of the bubble swarm trajectory in a jet bubbling reactor. *AIChE Journal*, *65*(5), 1–11.

Shuai, Y., Wang, X., Huang, Z., Yang, Y., Sun, J., Wang, J., & Yang, Y. (2019b). Bubble Size Distribution and Rise Velocity in a Jet Bubbling Reactor [Research-article]. *IECR*, *58*(41), 19271–19279.

Song, Y., Wang, D., Yin, J., Li, J., & Cai, K. (2019). Experimental studies on bubble breakup mechanism in a venturi bubble generator. *ANE*, *130*, 259–270.

Tabei, K., Haruyama, S., Y. (2007). Study of Micro Bubble Generation by a Swirl Jet. *JEE*, *2*(1), 172 – 182.

Terasaka, K., Hirabayashi, A., Nishino, T., Fujioka, S., & Kobayashi, D. (2011). Development of microbubble aerator for waste water treatment using aerobic activated sludge. *CES*, *66*(14), 3172–3179.

Vial, C., Camarasa, E., Poncin, S., Wild, G., Midoux, N., & Bouillard, J. (2000). Study of hydrodynamic behaviour in bubble columns and external loop airlift reactors through analysis of pressure fluctuations. *CES*, *55*(15), 2957–2973.

Wang, X., Shuai, Y., Zhang, H., Sun, J., Yang, Y., Huang, Z., … Yang, Y. (2020). Bubble breakup in a swirl-venturi microbubble generator. *CEJ*, *403*(February).

Wijayanta, S., Indarto, Deendarlianto, Catrawedarma, I. G. N. B., & Hudaya, A. Z. (2022). Statistical characterization of the interfacial behavior of the sub-regimes in gas-liquid stratified two-phase flow in a horizontal pipe. *FMI*, *83*(2), 102107.

Xiang, J., Li, Q., Tan, Z., & Zhang, Y. (2017). Characterization of the flow in a gas-solid bubbling fluidized bed by pressure fluctuation. *CES*, *174*, 93–103.

Xu, X., Ge, X. L., Qian, Y. D., Wang, H. L., & Yang, Q. (2018). Bubble-separation dynamics in a planar cyclone: Experiments and CFD simulations. *AIChE Journal*, *64*(7), 2689–2701.

Xu, X., Ge, X., Qian, Y., Zhang, B., Wang, H., & Yang, Q. (2018). Effect of nozzle diameter on bubble generation with gas self-suction through swirling flow. *CERD*, *138*, 13–20.

Yin, J., Li, J., Ma, Y., Li, H., Liu, W., & Wang, D. (2015). Study on the air core formation of a gas-liquid separator. *JFET of the ASME*, *137*(9), 1–9.

Yin, J., Qian, Y., Zhang, T., & Wang, D. (2018). Numerical investigation on the bubble separation in a gas-liquid separator applied in TMSR. *ANE*, *114*, 122–128.

Zhao, L., Sun, L., Mo, Z., Du, M., Huang, J., Bao, J., … Xie, G. (2019). Effects of the divergent angle on bubble transportation in a rectangular Venturi channel and its performance in producing fine bubbles. *IJMF*, *114*, 192–206.

Zhao, L., Sun, L., Mo, Z., Tang, J., Hu, L., & Bao, J. (2018). An investigation on bubble motion in liquid flowing through a rectangular Venturi channel. *ETFS*, *97*(October 2017), 48–58.